Journal of Southeast University (English Edition) Vol. 41, No. 1, pp. 44-50 Mar. 2025 ISSN 1003-7985

# Plateau frequency exploration of longitudinal guided waves for stress monitoring of steel strand

ZHANG Jing[1], LI Xuejian[1], LI Gang[1], YUAN Ye[2], YANG Dong[3]

(1. Department of Civil Engineering, Hefei University of Technology, Hefei 230009, China; 2. Department of Civil Engineering, The University of Hong Kong, Hong Kong 999077, China; 3. Earthquake Engineering Research & Test Center, Guangzhou University, Guangzhou 510006, China)

**Abstract**: To tackle the issue of notch frequency and center frequency drift of the L(0, 1) mode guided wave in ultrasonic guided wave-based stress monitoring of prestressed steel strands, a method using higher-order mode plateau frequencies is adopted. First, the correlation between group velocity peaks and phase velocities at these plateau frequencies is analyzed. This analysis establishes a quantitative relationship between phase velocity and stress in the steel strand, providing a theoretical foundation for stress monitoring. Then the two-dimensional Fourier transform is employed to separate wave modes. Dynamic programming techniques are applied in the frequency-velocity domain to extract higher-order modes. By identifying the group velocity peaks of these separated higher-order modes, the plateau frequencies of guided waves are determined, enabling indirect measurement of stress in the steel strand. To validate this method, finite element simulations are conducted under three scenarios. Results show that the higher-order modes of transient signals from three different positions can be accurately extracted, leading to successful cable stress monitoring. This approach effectively circumvents the issue of guided wave frequency drift and improves stress monitoring accuracy. Consequently, it significantly improves the application of ultrasonic guided wave technology in structural health monitoring.

**Key words**: steel strand; ultrasonic guided wave; plateau frequency; mode separation; stress monitoring

DOI: 10. 3969/j. issn. 1003-7985. 2025. 01. 006

Prestressed steel strands are vital components in suspension bridges and cable-stayed bridges, significantly affecting their durability, safety, and overall load-bearing capacity[1-2]. The advancement of ultrasonic guided wave technology has enhanced its use in defect detection and stress monitoring of pipelines and various structural elements[3-4]. However, the complex interaction between wires complicates the propagation mechanism of these waves in steel strands. Consequently, investigating the propagation of ultrasonic guided waves for stress monitoring of steel cables is crucial. In practical engineering, especially in low-frequency bands, the longitudinal L(0, 1) mode is preferred owing to its faster guided wave velocity compared to other modes at the same frequency. The "L" in L(0, 1) stands for "Longitudinal," indicating that the primary wave motion aligns with the wave propagation direction. Chen et al. [5] first established the relationship between stress and group velocity using the L(0, 1) mode, marking a pioneering effort in this approach. To effectively measure the tensile force in strands using guided waves, it is necessary to identify appropriate acoustic characteristic parameters that are highly sensitive to tensile force.

Although a large number of studies confirm the effectiveness of the L(0, 1) mode for stress measurement in steel strands, there are few studies on the higher-order modes, specifically L(0, $n$) when $n > 5$. These modes hold the potential for detecting damage in the steel strand[6-7]. Studies have shown that within a certain frequency range, higher-order mode shapes are concentrated in the rod center[8], leading to reduced energy leakage and increasingly comparable phase velocity variations. This frequency range is suitable for monitoring the stress levels in the steel strand[9].

The wave propagation properties in the frequency-wavenumber (f-k) domain highly depend on the wave frequency component and velocity. By recording time-domain signals at different propagation distances and applying the two-dimensional Fourier transform (2D-FFT)[10], it is possible to clearly distinguish each mode from the others within the f-k domain. Draudvilienė et al. [11] employed the 2D-FFT technique to identify spectral amplitude peaks at designated frequencies, demonstrating its effectiveness in detecting Lamb wave spectral peaks on aluminum plates through mathematical analysis and experimental validation. Michaels et al. [12] used f-k domain analysis to enhance acoustic field images for damage detection, efficiently separating time-domain waveforms by filtering out source wave signals to improve the visual

**Received** 2024-06-01, **Revised** 2024-08-21.

**Biographies**: Zhang Jing (1984—), female, doctor, associate professor; Yuan Ye (corresponding author), male, doctor, fredyhku@connect.hku. hk.

**Foundation item**: The National Natural Science Foundation of China (No. 52278303).

**Citation**: ZHANG Jing, LI Xuejian, LI Gang, et al. Plateau frequency exploration of longitudinal guided waves for stress monitoring of steel strand[J]. Journal of Southeast University (English Edition), 2025, 41(1): 44-50. DOI: 10. 3969/j. issn. 1003-7985. 2025. 01. 006.

clarity of defect scattering signals.

This study investigates the propagation characteristics of ultrasonic guided waves in isotropic circular rods under stress, focusing on the relationship between stress and group velocity curve peaks, particularly at higher-order mode frequencies, where phase velocity changes linearly with stress variations in steel strands. A method for monitoring stress in steel strands based on plateau frequencies is adopted. A numerical model is used to analyze guided wave propagation in multi-wire helical structures of tensioned steel strands. This method utilizes 2D-FFT to examine dispersion characteristics and applies ridge extraction techniques to filter excited multi-mode signals. It verifies the behavior of guided waves in stressed steel structures and their relationship with cable stress while addressing the effects of notch frequency and center frequency drift. The results demonstrate potential applications in structural health monitoring.

## 1 Propagation Characteristics of Guided Wave in Prestressed Waveguide

The study of acoustoelastic effects typically assumes that the waveguide medium material is hyperelastic, and it contains strain energy in the waveguide medium when subjected to a load. The strain energy function $U(E)$ of a superelastic body can be approximated as follows:

$$U(E) = \frac{1}{2!} c_{\alpha\beta\gamma\delta} E_{\alpha\beta} E_{\gamma\delta} + \frac{1}{3!} c_{\alpha\beta\gamma\delta\xi\eta} E_{\alpha\beta} E_{\gamma\delta} E_{\xi\eta} + \cdots \tag{1}$$

where $E$ is the Lagrangian strain tensor; $c_{\alpha\beta\gamma\delta}$ represents the second-order elastic parameters of the material; $c_{\alpha\beta\gamma\delta\xi\eta}$ denotes the third-order elastic parameters of the material; and subscripts $\alpha, \beta, \gamma, \delta, \xi, \eta$ indicate the coordinate direction in the reference configuration of the material.

Three deformation states of an object need to be considered when examining acoustic elasticity theoretically. The first state is the undeformed state or natural state, where there is no stress or strain. The second state is the initial state or predeformed state, where the object has already been subjected to deformation or prestressing. The third state is the final state or the state of ultrasonic guided wave detection when the object is predeformed based on superimposition of acoustic wavelet perturbations, which causes further deformation of the object. The position vectors of the above three states are denoted as $\boldsymbol{\zeta}$, $\boldsymbol{X}$, and $\boldsymbol{x}$. For simplicity, these vectors are expressed through their components $\zeta_\alpha (\alpha = 1, 2, 3)$, and $x_j (j = 1, 2, 3)$, respectively. The relationship between these vectors and their components is the following[13-15]:

$$X_J = X_J(\boldsymbol{\zeta}) = X_J(\zeta_1, \zeta_2, \zeta_3) \quad J = 1, 2, 3 \tag{2}$$

$$x_j = x_j(\boldsymbol{X}, t) = x_j(X_1, X_2, X_3, t) = x_j(\zeta_1, \zeta_2, \zeta_3, t) \quad j = 1, 2, 3 \tag{3}$$

When the natural state is transitioned to the initial state, the deformation is minor and static. The corresponding displacement of the mass point is represented by the vector $\boldsymbol{u}^{\text{in}}$; $\boldsymbol{u}^{\text{fi}}$ denotes the total displacement of the object in the final state; superscripts "in" and "fi" indicate the initial and final states corresponding to the strain tensor. The displacement from the natural state to the final state is represented by the vector $\boldsymbol{u}$. The relationship between these displacements can be expressed as follows:

$$\boldsymbol{X} = \boldsymbol{\zeta} + \boldsymbol{u}^{\text{in}} \tag{4}$$

$$\boldsymbol{x} = \boldsymbol{\zeta} + \boldsymbol{u}^{\text{fi}} = \boldsymbol{\zeta} + \boldsymbol{u}^{\text{in}} + \boldsymbol{u} \tag{5}$$

The displacement increment caused by small perturbations of acoustic waves superimposed on the object can be derived from the vector arithmetic relations:

$$\boldsymbol{u} = \boldsymbol{u}^{\text{fi}} - \boldsymbol{u}^{\text{in}} \tag{6}$$

The Lagrangian strain tensor for the initial state $E^{\text{in}}_{\alpha\beta}$ and final state $E^{\text{fi}}_{\alpha\beta}$ represented in natural coordinates are as follows[16]:

$$E^{\text{in}}_{\alpha\beta} = \frac{1}{2}\left( \frac{\partial u^{\text{in}}_\alpha}{\partial \zeta_\beta} + \frac{\partial u^{\text{in}}_\beta}{\partial \zeta_\alpha} + \frac{\partial u^{\text{in}}_\lambda}{\partial \zeta_\alpha} \frac{\partial u^{\text{in}}_\lambda}{\partial \zeta_\beta} \right) \tag{7}$$

$$E^{\text{fi}}_{\alpha\beta} = \frac{1}{2}\left( \frac{\partial u^{\text{fi}}_\alpha}{\partial \zeta_\beta} + \frac{\partial u^{\text{fi}}_\beta}{\partial \zeta_\alpha} + \frac{\partial u^{\text{fi}}_\lambda}{\partial \zeta_\alpha} \frac{\partial u^{\text{fi}}_\lambda}{\partial \zeta_\beta} \right) \tag{8}$$

where $u_\alpha$, $u_\beta$, and $u_\lambda$ in the initial and final states represent the natural coordinate components of $\boldsymbol{u}$; subscript $\lambda$ corresponds to subscripts $\alpha, \beta$ defined in Eq. (1), namely the direction of the coordinate. Assuming that the superimposed dynamic perturbations are small:

$$\| u_\alpha \| \ll \| u^{\text{in}}_\alpha \|, \ \| E^{\text{fi}}_{\alpha\beta} - E^{\text{in}}_{\alpha\beta} \| \ll \| E^{\text{in}}_{\alpha\beta} \| \tag{9}$$

Then, the strain tensor from the initial state to the final state can be approximated as

$$E_{\alpha\beta} = E^{\text{fi}}_{\alpha\beta} - E^{\text{in}}_{\alpha\beta} = \frac{1}{2}\left( \frac{\partial u_\alpha}{\partial \zeta_\beta} + \frac{\partial u_\beta}{\partial \zeta_\alpha} + \frac{\partial u^{\text{in}}_\lambda}{\partial \zeta_\alpha} \frac{\partial u_\lambda}{\partial \zeta_\beta} + \frac{\partial u^{\text{in}}_\lambda}{\partial \zeta_\beta} \frac{\partial u_\lambda}{\partial \zeta_\alpha} \right) \tag{10}$$

In the initial state, the stress at a point can be expressed using the Cauchy stress component, denoted as $t^{\text{in}}_{JK}$, where subscripts $J$ and $K$ indicate the stress component in the $J$ direction acting on the face in the $K$ direction in the current configuration. The Piola-Kirchhoff stress, defined in natural coordinates, is expressed as $T^{\text{in}}_{\alpha\beta}$. The relationship between the two tensors is as follows:

$$t^{\text{in}}_{JK} = \frac{1}{J^{\text{in}}} \frac{\partial X_K}{\partial \zeta_\beta} \frac{\partial X_J}{\partial \zeta_\alpha} T^{\text{in}}_{\alpha\beta} \tag{11}$$

According to Eq. (4):

$$\frac{\partial X_K}{\partial \zeta_\beta} = \delta_{K\gamma}\left( \delta_{\gamma\beta} + \frac{\partial u^{\text{in}}_\lambda}{\partial \zeta_\beta} \right) \tag{12}$$

where $J^{\text{in}} = \left| \frac{\partial \boldsymbol{X}}{\partial \zeta} \right|$ indicates the determinant of the matrix $(J, \alpha = 1, 2, 3)$; $\delta_{K\gamma}$ and $\delta_{\gamma\beta}$ are Kronecker notations.

For hyperelastic bodies, the relationship between the Biola-Kirchhoff stress $T_{\alpha\beta}$ and the strain potential energy function $U(E)$ is as follows:

$$T_{\alpha\beta} = \frac{\partial U}{\partial E_{\alpha\beta}} \tag{13}$$

The acoustoelastic equation for a solid medium with density $\rho^{\text{o}}$ in the natural coordinate system is given by

$$\frac{\partial}{\partial \zeta_\beta}\left( T^{\text{in}}_{\alpha\beta} \frac{\partial u_\alpha}{\partial \zeta_\lambda} + \Gamma_{\alpha\beta\gamma\delta} \frac{\partial u_\gamma}{\partial \zeta_\delta} \right) = \rho^{\text{o}} \frac{\partial^2 u_\alpha}{\partial t^2} \tag{14}$$

$$\Gamma_{\alpha\beta\gamma\delta} = c_{\alpha\beta\gamma\delta} + c_{\alpha\beta\lambda\delta} \frac{\partial u^{\text{in}}_\gamma}{\partial \zeta_\lambda} + c_{\lambda\beta\gamma\delta} \frac{\partial u^{\text{in}}_\alpha}{\partial \zeta_\lambda} + c_{\alpha\beta\gamma\delta\xi\eta} e^{\text{in}}_{\xi\eta} \tag{15}$$

The acoustoelastic equation in the initial coordinate system can be expressed as follows:

$$\frac{\partial}{\partial X_J}\left[ (\delta_{IK} t^{\text{in}}_{JL} + C_{IJKL}) \frac{\partial u_K}{\partial X_L} \right] = \rho^{\text{in}} \frac{\partial^2 u_I}{\partial t^2} \tag{16}$$

$$C_{IJKL} = c_{IJKL}(1 - e^{\text{in}}_{NN}) + c_{IJKLMN} e^{\text{in}}_{MN} + c_{MJKL} \frac{\partial u^{\text{in}}_I}{\partial X_M} + c_{IMKL} \frac{\partial u^{\text{in}}_J}{\partial X_M} + c_{IJML} \frac{\partial u^{\text{in}}_K}{\partial X_M} + c_{IJKM} \frac{\partial u^{\text{in}}_L}{\partial X_M} \tag{17}$$

where $e_{MN}$ represents a small strain; $e_{NN} = e_{11} + e_{22} + e_{33}$; the value of $C_{IJKL}$ depends on the material properties and the initial displacement field, known as equivalent stiffness, where subscripts $I$, $J$, $K$, $L$, $M$ and $N$ indicate the direction of the coordinate in the initial configuration.

Based on the above theory, the body wave velocity equation in the initial coordinate system can be expressed as follows[17].

The longitudinal wave propagating along the stress direction is expressed as follows:

$$c^{\sigma}_{\text{L}} = \sqrt{\frac{\lambda + 2\mu}{\rho} + \frac{\sigma}{3\rho K_0}\left[ \frac{\lambda + \mu}{\mu}(4\lambda + 10\mu + 4m) + \lambda + 2l \right]} \tag{18}$$

and the longitudinal wave propagating perpendicular to the direction of stress:

$$c^{\sigma}_{\text{T}} = \sqrt{\frac{\lambda + 2\mu}{\rho} + \frac{\sigma}{3\rho K_0}\left[ 2l - \frac{2\lambda}{\mu}(\lambda + 2\mu + m) \right]} \tag{19}$$

where $\sigma$ is the axial stress, the bulk modulus $K_0 = \lambda + \frac{2}{3}\mu$; $\lambda$ and $\mu$ are the Lame constants; $l$, $m$ and $n$ denote the third-order elastic constant.

## 2 Steel Strand Stress Monitoring Method Based on Plateau Frequency

The stable stress dependence near their peak group velocity offers a new approach for stress monitoring in the steel strand by utilizing higher-order modes. In addition, using the linear stress dependence predicted by the rod theory, the influence of stress on the phase velocity of the guided wave mode in the steel strand can be predicted using acoustic elasticity theory.

As shown in Fig. 1, the dispersion curves for a circular rod with a diameter of 5 mm are labeled with peak group velocity and plateau phase velocity of each mode, and each peak velocity corresponds to a specific plateau frequency. By determining the plateau frequency from the peak group velocity, the plateau phase velocity at that frequency can then be identified. However, high convergence is only observed in the high-mode plateau phase velocity region. By separating the single mode of ultrasonic guided waves, the group velocity and corresponding frequency of each mode can be obtained.

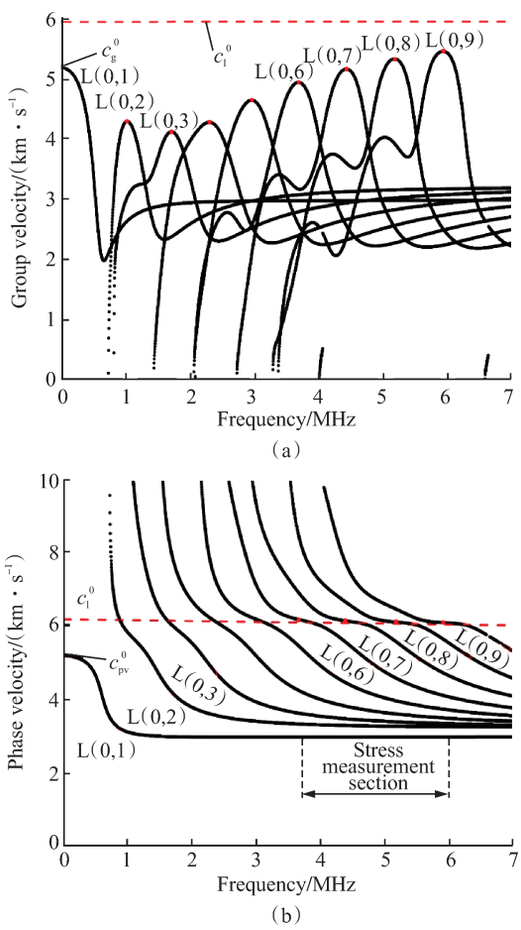


**Fig. 1** Theoretical dispersion curve of the circular rod. (a) Group velocity curve; (b) Phase velocity curve

The phase velocity of the steel strands in the stress-free state is $c^0_{\text{pv}}$. When the axial stress changes, the phase velocity becomes $c^0_{\text{pv}} + \Delta c_{\text{pv}}$. A linear relationship exists between the change in stress and the change in phase velocity as follows[18]:

$$\Delta c_{\text{pv}} = \kappa_{\text{pv}} \Delta\sigma \tag{20}$$

where $\kappa_{\text{pv}}$ is an acoustoelastic constant coefficient that can be calculated according to the following equation:

$$\kappa_{pv} \approx \kappa_1 = \frac{(\lambda + 2l)\mu + (2\lambda + 6\mu + 4m)(\lambda + \mu)}{2\mu(3\lambda + 2\mu)\sqrt{\rho(\lambda + 2\mu)}} \quad (21)$$

where $\kappa_1$ is the acoustoelastic constant, and the physical meaning of the other parameters can be referred to in Section 1, and their values can be determined by the material properties. For materials with established acoustic parameters, the longitudinal and transverse ultrasonic waves under different stress states can be calculated using numerical algorithms. The acoustic and mechanical parameters for steel, as provided by Chen et al. [19], can be used in this context. Once the acoustoelastic constant is determined, changes in stress $\Delta\sigma$ can be derived from alterations in phase velocity $\Delta c_{pv}$. The phase velocity of a single mode can be calculated by measuring the waveform phase time variation $\Delta t_p$ as follows:

$$\Delta c_{pv} = -\frac{(c_{pv}^0)^2}{d}\Delta t_p \quad (22)$$

where $d$ is the stress propagation distance. From Eqs. (20) and (21), the following is obtained:

$$\Delta\sigma = -\frac{(c_{pv}^0)^2}{k_1 d}\Delta t_p \quad (23)$$

The phase velocity $c_{pv}^0$ of the structure in the stress-free state is equal to the longitudinal wave velocity $c_1^0$. Therefore, the above equation can be rewritten as follows:

$$\Delta\sigma = -\frac{(c_1^0)^2}{k_1 d}\Delta t_p \quad (24)$$

## 3 Excitation and Separation of Multimodes of Steel Strand

The finite element model of the steel strand is used to obtain the required time-domain signals. Following this, the mode extraction and separation of the higher-order longitudinal mode are carried out. To accurately monitor the stress in the prestressed steel strand, the modelling and parameter selection should be based on satisfying the acoustoelastic effect.

### 3.1 Finite element model

The steel strands consist of seven wires, with the core wire surrounded by six others. This study uses the ABAQUS/Explicit software to simulate a finite element model of the steel strand with the length $L$ of 480 mm, the nominal diameter $D$ of 15.7 mm and the pitch $\rho_h$ of 240 mm.

To ensure accurate spatial and temporal resolution in the simulation results, specific criteria for mesh size and time increments should be satisfied. The frequency band selected for analysis is within the maximum frequency $f_{max}$= 4 MHz, aiming to minimize the effects of mode separation in higher frequency bands. The maximum mesh length should meet the following requirements:

$$L_{max} = \frac{\lambda_{min}}{8-1} = \frac{c_T^\sigma / f_{max}}{7} = 0.115 \text{ mm} \quad (25)$$

where $\lambda_{min}$ denotes the shortest wavelength. Therefore, the minimum axial element size of the steel strands is 0.1 mm, while the element type is defined as C3D8R (three-dimensional stress 8-node linear hexahedron element, simplified integral). The mesh results are illustrated in Fig. 2.

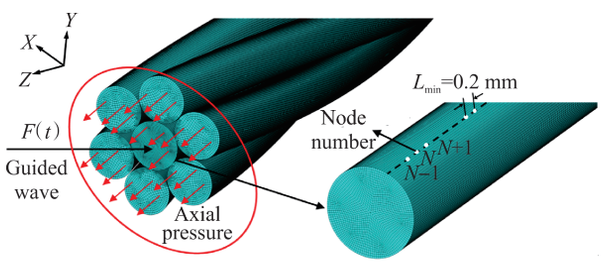


**Fig. 2** Mesh division of the steel strand

The sensitivity of the guided wave to stress in finite element simulations of the steel strand under axial tension is influenced by the duration of continuous excitation. To address this, the simulation is divided into three stages: applying axial tension, activating the excitation source, and propagating the guided wave. This method prevents the disruption of guided wave propagation owing to instantaneous tension, allowing the wave to propagate after the strand stabilizes under axial force. The analysis uses a fully automatic integration time step.

In scenarios where the steel strand is subjected to axial tension, finite slip surface contact simulates extrusion and sliding friction between the steel wires, while penalty contact ensures that different steel wire units do not penetrate each other. The contact between normal steel wires is set as hard contact, while tangential friction is modeled using the penalty friction formula, with a friction coefficient of 0.6. At one end of the model, all wires are fixed with no displacement and rotation, while the other end releases only axial displacement. Initially, tension is applied at the end of releasing axial displacement to simulate axial tension, with a force of 1 116 MPa. In the second step, guided wave propagation is simulated under stable axial force by applying a broadband concentrated Rick wave at the tensile end. The time-frequency domain curve of the excitation signal is shown in Fig. 3. Its peak frequency is near 1.4 MHz, covering a frequency range from 0 to 4 MHz.

A signal acquisition point is set every 0.1 mm along the axial direction of the center bar of the steel strands at the excitation end, resulting in a total of 2 400 points to form a space-time matrix. The axial acceleration time-do-

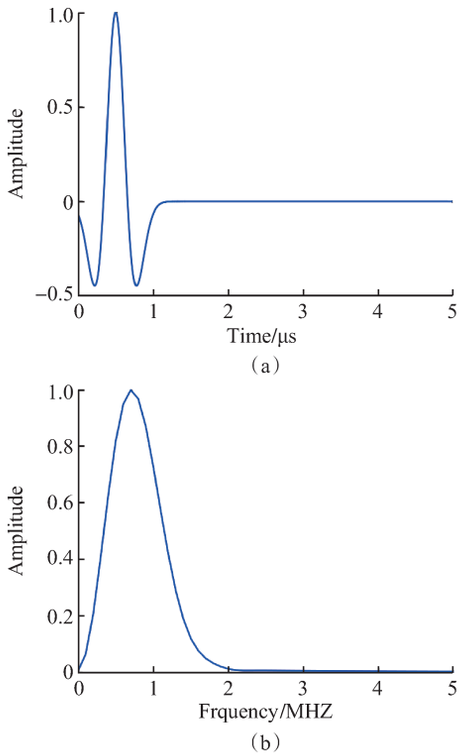


**Fig. 3** Ricker wavelet excitation signal. (a) Time-domain waveform; (b) Spectrum waveform

main signals from each node are extracted and analyzed using 2D-FFT to derive the dispersion curve within the frequency range of excitation. Fig. 4 depicts the normalized signal amplitude diagram of transient acceleration at

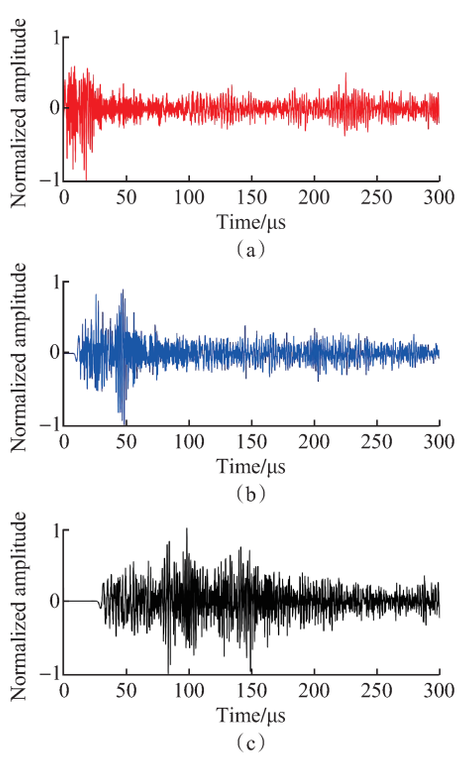


**Fig. 4** Normalized signal amplitude of the transient acceleration signal at the position located a distance $x_1$ from the excitation end. (a) $x_1$ = 100 mm; (b) $x_1$ = 200 mm; (c) $x_1$ = 300 mm

three different positions within the core of the receiving steel strands. This figure reveals that multiple mode superpositions make it difficult to identify modes based solely on time-domain signals.

### 3.2 Acquisition of platform frequency

The 2D-FFT is applied to the space-time matrix derived from axial transient acceleration signals along the center bar of the steel strands, resulting in the f-k curve depicted in Fig. 5. When axial force is exerted, the surrounding wire rope exerts a torsional force on the central rod, altering guided wave propagation, as shown by the applied load force. Analysis of the figure reveals that the longitudinal mode predominantly carries energy, displaying multiple modes simultaneously, each exhibiting distinct dispersion characteristics compared to single-line waveguides.

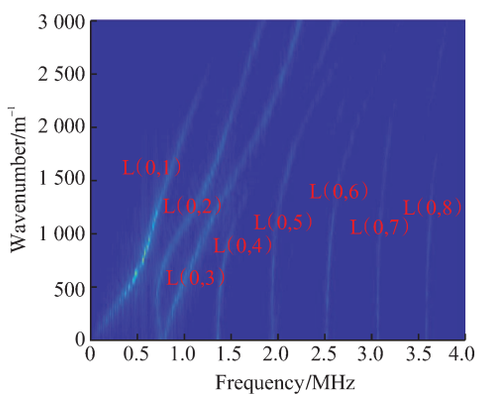


**Fig. 5** Frequency-wavenumber curve corresponding to 60% of ultimate tensile strength

The f-k domain dispersion curves of the steel strands are extracted from the ridges using dynamic programming[20], as shown in Fig. 6(a). As evident in the figure, the first four modes of energy ridges are identified, but owing to spectral noise, higher-order mode ridges are less clear. However, the overall result is not affected by the change of the position of a small part of the ridge line. According to its position, f-k signal points can be recorded in a certain area around the ridge line. Multi-mode f-k domains are separated based on ridge extraction results, as shown in Figs. 6(b)-(e), successfully isolating the first four modes. The separated single mode stands out visually, unaffected by the other modes, while the remaining modes appear brighter in the f-k domain.

A particular mode can be isolated from the multi-modal signal of the strand to determine the group velocity at a specific frequency. By associating the peak group velocity with the phase velocity at the platform frequency, it is possible to infer the correlation between phase velocity change and stress within the strand.

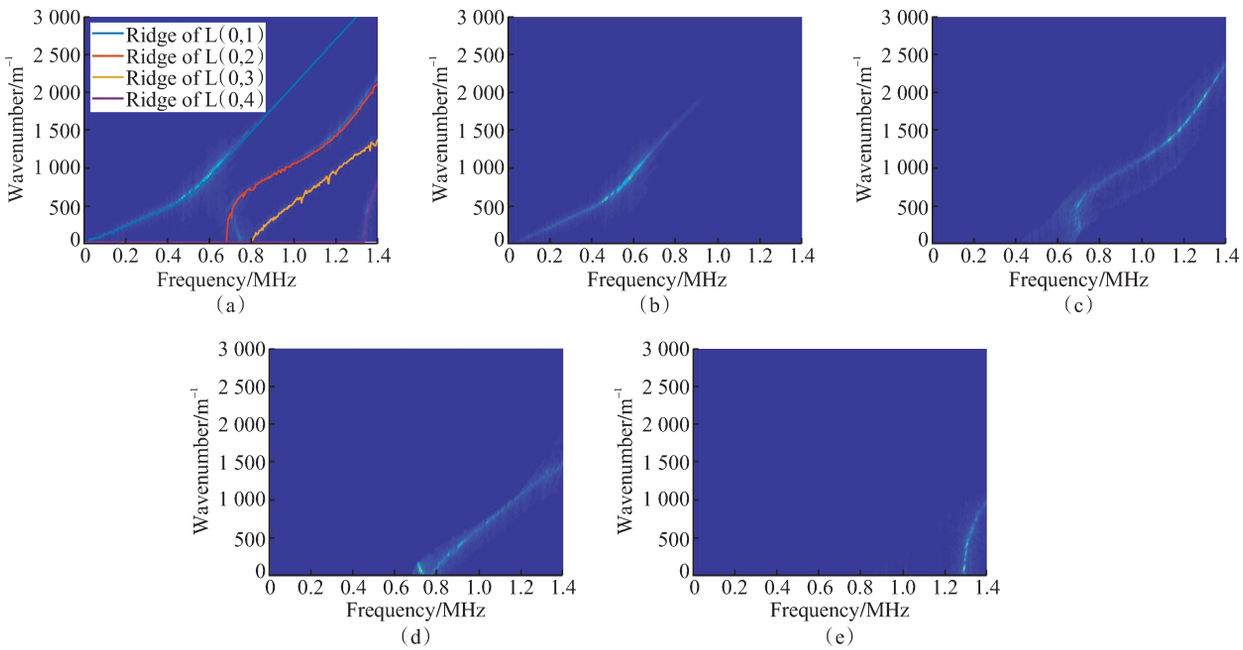


**Fig. 6** Ridge extraction results of the steel strands. (a) Multi-order mode ridge extraction; (b) L(0,1) ridge separation; (c) L(0,2) ridge separation; (d) L(0,3) ridge separation; (e) L(0,4) ridge separation

## 4 Conclusions

(1) The research established a quantitative relationship between phase velocity and stress in steel strands. By analyzing the correlation between group velocity peaks and phase velocities at plateau frequencies, a theoretical basis for stress monitoring was provided. Results show that, at higher-order mode frequencies, there is a linear relationship between the phase velocity change and the stress change of the steel strand.

(2) A new method for separating guided wave modes was developed using 2D-FFT to convert signals into the frequency-wavenumber domain, coupled with dynamic programming to extract higher-order modes. This approach successfully separated the first four modes (L(0, 1) to L(0,4)) from a complex multi-mode signal.

(3) A novel stress monitoring approach was adopted using plateau frequencies of guided waves. By associating group velocity peaks to phase velocities at these plateau frequencies, the stress in steel strands can be indirectly measured. This method effectively minimizes the influence of guided wave frequency drift and improves stress monitoring accuracy.

## References

[1] MAO J X, KE X D, SU X, et al. Fatigue performance analysis of suspenders of a long span suspension bridge under monitored traffic flow [J]. Journal of Southeast University (Natural Science Edition), 2024, 54(4): 952-960. (in Chinese)

[2] TAO T Y, GAO W J, JIANG Z X, et al. Analysis on wind-induced vibration and its influential factors of long suspenders in the wake of bridge tower [J]. Journal of Southeast University (Natural Science Edition), 2023, 53(6): 1065-1071. (in Chinese)

[3] WAN S P, FANG Z F, ZHOU H J, et al. Experimental study on static tensile and acoustic emission monitoring of corroded steel wires and cables [J]. Journal of Southeast University (Natural Science Edition), 2024, 54(3): 567-577. (in Chinese)

[4] CHEN X H, XU J, LI Y, et al. Characteristic parameters of magnetostrictive guided wave testing for fatigue damage of steel strands [J]. Materials, 2023, 16(15): 5215.

[5] CHEN H L R, HE Y D, GANGARAO H V. Measurement of prestress force in the rods of stressed timber bridges using stress waves [J]. Materials Evaluation, 1998, 56(8): 977-981.

[6] LAGUERRE L, TREYSSEDE F. Non destructive evaluation of seven-wire strands using ultrasonic guided waves [J]. European Journal of Environmental and Civil Engineering, 2011, 15(4): 487-500.

[7] ŠEŠTOKĖ J, JASIŪNIENĖ E, ŠLITERIS R, et al. Exciting and detecting higher-order guided lamb wave modes in high-density polyethylene structures using ultrasonic methods [J]. Materials, 2023, 17(1): 163.

[8] ERVIN B L, KUCHMA D A, BERNHARD J T, et al. Monitoring corrosion of rebar embedded in mortar using high-frequency guided ultrasonic waves [J]. Journal of Engineering Mechanics, 2009, 135(1): 9-19.

[9] PAVLAKOVIC B N, LOWE M J S, CAWLEY P. High-frequency low-loss ultrasonic modes in imbedded bars [J]. Journal of Applied Mechanics, 2001, 68(1): 67-75.

[10] AERON S, BOSE S, VALERO H P. Joint multi-mode dispersion extraction in frequency-wavenumber and space-time domains [J]. IEEE Transactions on Signal Processing, 2015, 63(15): 4115-4128.

[11] DRAUDVILIENĖ L, MEŠKUOTIENĖ A, RAIŠUTIS

R, et al. Accuracy assessment of the 2D-FFT method based on peak detection of the spectrum magnitude at the particular frequencies using the lamb wave signals[J]. Sensors, 2022, 22(18): 6750.
[12] MICHAELS T E, MICHAELS J E, RUZZENE M. Frequency-wavenumber domain analysis of guided wavefields[J]. Ultrasonics, 2011, 51(4): 452-466.
[13] AGGELIS D G, KLEITSA D, IWAMOTO K, et al. Elastic wave simulation in ground anchors for the estimation of pre-stress[J]. Tunnelling and Underground Space Technology, 2012, 30: 55-63.
[14] THOMSON W T. Transmission of elastic waves through a stratified solid medium[J]. Journal of Applied Physics, 1950, 21(2): 89-93.
[15] KNOPOFF L. A matrix method for elastic wave problems [J]. Bulletin of the Seismological Society of America, 1964, 54(1): 431-438.
[16] PAO Y H, SACHSE W, FUKUOKA H. Acoustoelasticity and ultrasonic measurements of residual stresses[J]. Physical Acoustics, 1984, 17: 61-143.
[17] ROSE J L, NAGY P B. Ultrasonic waves in solid media [J]. The Journal of the Acoustical Society of America, 2000, 107(4): 1807-1808.
[18] DUBUC B, EBRAHIMKHANLOU A, SALAMONE S. Higher order longitudinal guided wave modes in axially stressed seven-wire strands[J]. Ultrasonics, 2018, 84: 382-391.
[19] CHEN H L R, WISSAWAPAISAL K. Measurement of tensile forces in a seven-wire prestressing strand using stress waves [J]. Journal of Engineering Mechanics, 2001, 127(6): 599-606.
[20] LI G, ZHANG J, CHENG J K, et al. Multi-order mode excitation and separation of ultrasonic guided waves in rod structures using 2D-FFT [J]. Sensors, 2023, 23 (20): 8483.

# 钢绞线应力监测的纵向超声导波平台频率获取

张静[1], 李雪健[1], 李刚[1], 袁冶[2], 杨栋[3]

(1.合肥工业大学土木工程学院,合肥 230009;2.香港大学土木工程学院,香港 999077;
3.广州大学工程抗震研究中心,广州 510006)

**摘要:** 通过研究超声导波在预应力钢绞线应力监测中遇到的L(0,1)模态导波缺口频率及陷频中心漂移的问题,提出一种基于高阶模态平台频率的应力监测方法。首先分析群速度峰值与平台频率处相速度的关联特性,建立了相速度与钢绞线应力之间的定量关系,为应力监测提供理论依据;接着采用二维傅里叶变换对导波模态进行分离,在频率-波速域应用动态规划技术提取高阶模态,通过分离后的高阶模态群速度峰值确定导波平台频率,实现钢绞线应力间接测量;最后,基于有限元模型验证了3种不同工况下所提平台频率选取方法的有效性。结果表明,利用3个不同位置的瞬态信号均能从中准确提取高阶模态并实现应力监测,且可有效避免导波频率漂移的影响,提高监测准确性,有助于增强超声导波技术在结构健康监测中的应用效果。

**关键词:** 钢绞线;超声导波;平台频率;模态分离;应力监测
**中图分类号:** U448